Polarization observations of nine southern millisecond pulsars

R. N. Manchester

Australia Telescope National Facility, CSIRO, PO Box 76, Epping NSW 1710, Australia

Dick.Manchester@csiro.au

and

J. L. Han

National Astronomical Observatories, Chinese Academy of Sciences, Beijing 100012, China

hjl@bao.ac.cn

ABSTRACT

Mean pulse profiles and polarization properties are presented for nine southern pulsars. The observations were made using the Parkes radio telescope at frequencies near 1330 MHz; three of the nine pulsars were also observed at 660 MHz. A very high degree of circular polarization was observed in PSR J1603−7202. Complex position angle variations which are not well described by the rotating-vector model were observed in PSRs J2124−3358 and J2145−0750, both of which have very wide profiles. Rotation measures were obtained for all nine pulsars, with two implying relatively strong interstellar magnetic fields.

Subject headings: Pulsars: general — polarization — ISM: magnetic field

1. Introduction

Observations of the polarization of mean pulse profiles have given much information about the pulsar radio emission mechanism. Pulsars often have very high linear polarization and the sweep of position angle across the pulse is generally well described by the rotating-vector model (Radhakrishnan & Cooke 1969; Komesaroff 1970). This and the bilateral symmetry of many pulse profiles led to a model in which the emission is beamed into a hollow cone centered on the magnetic axis. With observations of an increasing number of pulsars it soon became clear that the mean pulse profiles of many pulsars were more complex. The frequent occurence of a central emission peak (Backer 1976) led to the idea

of a 'core' component in contrast to the outer 'conal' components. Further observations showed that many pulsars had multiple conal components leading to ideas of multiple cones (Rankin 1993; Kramer et al. 1994; Mitra & Deshpande 1999) or patchy beams (Lyne & Manchester 1988; Han & Manchester 2001). Core emission tends to have a steeper spectrum than conal emission and a higher degree of circular polarization, often with a reversal of sense near the profile center (Rankin 1983; Lyne & Manchester 1988), although reversing circular polarization is sometimes observed in conal emission (Han et al. 1998). The apparent width of both core and conal beams is a function of pulse period (P), with an approximate $P^{-1/2}$ dependence (Rankin 1990; Biggs 1990).

With the discovery of millisecond pulsars (MSPs), the parameter ranges available for study of pulse emission processes was greatly extended. MSPs have much weaker surface magnetic fields than 'normal' pulsars, with B_0 typically a few by 10^8 G, compared to 10^{12} G for normal pulsars. They also have much smaller magnetospheres, conventionally defined to be limited by the light cylinder at radius $R_{LC} = cP/2\pi$, where P is the pulsar period and c is the velocity of light. For the fastest MSP, PSR B1937+21, R_{LC} is only 74 km, or about ten times the neutron star radius. One would therefore expect the radio emission from MSPs to be rather different to that from normal pulsars. MSP pulse profiles are generally wider (in pulse phase) than those of normal pulsars, which is not surprising in view of the wider angle subtended by the 'open' field lines which penetrate the light cylinder and define the extent of the polar cap. Also, MSP profiles have different frequency evolution characteristics compared to most normal pulsars. In particular, the component separations are largely independent of frequency (Kramer et al. 1999a). It is not clear that the distinctions and relationships between 'core' and 'conal' emission seen in longer-period pulsars apply to MSPs. For example, the strong component in PSR J0437−4715 is clearly central to the emission beam but has a flatter spectrum than the outer components (Navarro et al. 1997).

Despite these differences, there are many similarities in the radio emission properties of MSPs and normal pulsars. If the greater width of MSP profiles is ignored, the shapes of MSP mean pulse profiles are very similar to those of normal pulsars. However, among the MSPs, there is a greater proportion of 'interpulse' profiles, with two main regions of pulse emission separated by approximately 180° of pulse phase or longitude. MSP profiles often appear to have more components than normal pulsars, but Kramer et al. (1998) have argued that this is simply because MSP components are more obvious because of their wider spacing. On average, the radio emission of MSPs has a spectral index which is only marginally steeper than that of normal pulsars and may in fact be the same (Toscano et al. 1998; Kramer et al. 1998). MSPs are typically somewhat less luminous than normal pulsars but there is a large overlap in the luminosity distributions. Finally, the polarization properties of MSPs and normal pulsars are remarkably similar, with both often having high fractional

linear polarization and generally smaller levels of circular polarization. Orthogonal jumps in position angle are seen in both classes of pulsar (e.g. Stinebring et al. 1984; Thorsett & Stinebring 1990). Variations of position angle (PA) through MSP profiles are often more complex than is typical for normal pulsars. Despite this, in many cases the PA can be approximately fitted by the simple rotating vector model (RVM) which applies to most normal pulsars, at least once orthogonal jumps are taken into account (e.g. Arzoumanian et al. 1996). These similarities leave little doubt that the basic radio emission mechanism is the same in normal pulsars and MSPs.

Extensive studies of the polarization properties of MSPs have previously been made by Thorsett & Stinebring (1990): PSRs B1937+21, B1953+29 and B1957+20 at several frequencies between 430 and 2830 MHz; Navarro et al. (1997): PSR J0437−4715 at 438, 660 and 1512 MHz; Arzoumanian et al. (1996): PSR B1534+12 at 430 MHz; Xilouris et al. (1998): 24 pulsars at 1410 MHz; Stairs, Thorsett & Camilo (1999): 19 pulsars at 410, 610 and/or 1414 MHz; and Lommen et al. (2000): PSR J0030+0451 at 430 MHz. All observations except those of PSR J0437−4715 by Navarro et al. were made using northern hemisphere telescopes, so there is little information on the polarization of the southern MSPs. Also, there are significant discrepancies in the results of different groups for some pulsars. For example, results from Xilouris et al. (1998) and Stairs et al. (1999) for PSRs J1022+1001, J1713+0747 and J2145-0750 at frequencies near 1400 MHz differ substantially.[1] It is important to understand whether these differences are due to time variations such as mode changing (Kramer et al. 1999b) or problems with data processing and/or calibration. Furthermore, in some previous studies (e.g. Stairs et al. 1999) the position angle scale is not absolute. Absolute position angles are important for Faraday rotation studies and in comparisons with other properties. Important examples are the comparison of the pulsar rotation axis direction implied by radio polarization measurements with that deduced from X-ray observations and with the direction of the pulsar proper motion. (Helfand et al. 2001; Radhakrishnan & Deshpande 2001).

With their high linear polarization, it is relatively easy to determine rotation measures (RMs) for most pulsars. Combined with the dispersion measure (DM), pulsars give a direct measure of the mean line-of-sight magnetic field between the Sun and the pulsar, weighted by the local electron density. Since the DM also provides an estimate of the pulsar distance, pulsars are a valuable probe of the Galactic magnetic field (e.g. Han et al. 2002). Most MSPs are relatively close to the Sun, so they provide information on conditions in the local region of the Galaxy.

[1]Stairs et al. (1999) use a convention for sense of position angle which is opposite to the astronomical convention used by other authors.

We have used the Parkes 64-m telescope of the Australia Telescope National Facility and the Caltech pulsar correlator to make observations of nine southern MSPs at 20 cm and, for three of these, at 50 cm. Five of these pulsars have no previously published polarization observations and none have previously published rotation measures. Details of the observing system and observational parameters are given in § 2. The polarization and RM results are presented in § 3 and § 4 respectively, and in § 5 we discuss some implications of our polarization measurements.

2. Observations

Observations were made in three sessions, 1996 August 31 – September 5, 1999 December 12 – 17, and 2000 December 14 – 19 using the Parkes 64-m radio telescope. The 20-cm observations were made using the central beam of the Parkes multibeam receiver (Staveley-Smith et al. 1996) in the 1999 and 2000 sessions with a central frequency of 1318.5 MHz. This system has cryogenically cooled preamplifiers, giving a system temperature of about 21 K or about 29 Jy, and orthogonal linear feeds with a calibration signal injected at angle of 45° to the feed probes. Because this system has significant cross-coupling between the feed probes, all observations were made at two feed angles at ±45°. These measurements were summed after compensation for the feed rotation, thereby eliminating most of the effects of feed cross-coupling. The 50-cm observations had a central frequency of 660 MHz and were were made in the 1996 and 2000 sessions using a receiver with cryogenically cooled preamplifiers and a cavity-backed disk feed, again with a calibration signal injected at 45°. Observations with this system were made at fixed feed angle; in this case the feed cross-coupling is small and did not significantly affect the polarization results. The flux scale was established using observations of Hydra A, assumed to have flux densities of 85 and 45 Jy at 660 and 1320 MHz, respectively.

The Caltech correlator system (Navarro 1994) was used to form the polarization products and to bin the signals synchronously with the pulsar period. For both 660 and 1320 MHz, the signals were up-converted to 1580 MHz, band-limited to 32 or 128 MHz respectively and power levels adjusted for 2-bit digitization at 256 MHz. The correlator gives 128 lags in each of four polarization channels and folds the data synchronously with the pulsar period with 1024 bins per period. After on-line folding, typically for 90 seconds, the 512 sub-integration profiles were transferred to a workstation for further processing. Data in each phase bin were transformed to the frequency domain and narrow-band interference rejected. Using a pulsed calibration observation made immediately before each pulsar observation, the data were corrected for differential delays between the two polarization channels and

calibrated into mJy units. After conversion to Stokes parameters, the data were corrected for parallactic angle rotation and ionospheric Faraday rotation and dedispersed to form 16 to 64 frequency sub-bands, depending on the pulsar DM.

In off-line analysis, the orthogonal observation pairs for 1320 MHz were summed and the data were summed in time to form Stokes-parameter profiles for each sub-band. In most cases several observation pairs were summed to form the final profiles. Because of low system gain, some sub-bands at one or both ends of the bandpass were normally rejected, changing the effective center frequency. We then summed the data in frequency for a range of trial RMs, (normally in a range of ± 1500 rad m^2 with a step of 25 rad m^2) to search for a peak in the linearly polarized intensity $L = (Q^2 + U^2)^{1/2}$. Stokes parameter profiles were then formed for the upper and lower halves of the bandpass, correcting for the approximate RM determined in the previous stage of analysis. The best estimate of pulsar RM was then obtained by taking weighted means of position-angle (PA) differences for bins where the uncertainty in the PA difference was less than 10°. Finally, a single set of Stokes-parameter profiles was formed for each observation.

Table 1 lists the basic observational parameters for the nine observed MSPs. Columns are, in order: pulsar name based on J2000 coordinates, pulse period, DM, year(s) in which the observations were made, effective center frequency and bandwidth after sub-band rejection, number of bins across the pulse period and the total observation time.

3. Results

The results are presented in terms of Stokes I (total intensity), linearly polarized intensity L and Stokes V, defined in the sense $I_L - I_R$, where I_L and I_R are the left- and right-circularly polarized intensities respectively according to the IRE definition. The linear position angle is measured from north toward east (counter-clockwise) on the sky, in the normal astronomical convention. Table 2 gives a summary of the results. Columns are, in order: pulsar name, mean flux density, fractional linear polarization, fractional net circular polarization, fractional absolute circular polarization, estimated error in the fractional polarizations, pulse width at 50% of the peak in degrees (where the pulse period = 360°) and milliseconds, and pulse width at 10% of the peak in degrees and milliseconds. The mean flux density S is the sum of I across the profile divided by the number of bins per period, and the fractional polarizations are the sum of the polarization quantity (L, V or $|V|$) across the pulse profile divided by the sum of I across the profile.

In the following subsections we present polarization profiles and discuss each pulsar in

Table 1: Observational parameters for southern millisecond pulsars

PSR	P (ms)	DM ($cm^{-3}pc$)	Obs. Date	Ctr Freq. (MHz)	BW (MHz)	Nr of Bins	Obs. time (s)
J0613−0200	3.062	38.79	99+00	1335	96	64	3960
J0711−6830	5.491	18.41	99+00	1335	96	128	5580
J1045−4509	7.474	58.15	99	1335	96	128	2700
J1603−7202	14.842	38.05	96	661	24	128	1800
			99	1327	96	256	2700
J1623−2631	11.076	62.86	00	1331	96	128	1080
J1643−1224	4.622	62.41	00	1331	96	64	1080
J2124−3358	4.931	4.62	00	659	24	256	2160
			99+00	1327	80	128	11520
J2129−5721	3.726	31.85	96	659	24	64	2880
			99	1331	96	128	2880
J2145−0750	16.052	9.00	00	1335	96	256	2160

Table 2: Polarization and pulse width parameters for southern millisecond pulsars

PSR	Freq. (MHz)	S (mJy)	$\langle L\rangle/S$ (%)	$\langle V\rangle/S$ (%)	$\langle\|V\|\rangle/S$ (%)	σ (%)	W_{50} (°)	W_{50} (ms)	W_{10} (°)	W_{10} (ms)
J0613−0200	1335	4.6	15	2	4	1	67	0.57	130	1.11
J0711−6830	1335	2.1	13	−16	19	2	125	1.90	175	2.68
J1045−4509	1335	2.4	14	14	17	2	40	0.82	78	1.62
J1603−7202	661	21.6	13	30	30	1	38	1.57	63	2.59
	1327	7.0	13	29	30	1	33	1.34	49	2.02
J1623−2631	1331	1.4	34	1	18	3	19	0.57	88	2.71
J1643−1224	1331	5.1	7	−1	11	1	47	0.60	114	1.47
J2124−3358	659	130	41	−5	9	1	169	2.32	330	4.52
	1327	7.9	29	−1	6	1	37	0.51	278	3.82
J2129−5721	659	6.8	50	−28	30	2	46	0.47	113	1.17
	1331	1.4	45	−28	31	2	30	0.31	83	0.86
J2145−0750	1335	16.6	15	7	9	1	8.5	0.38	94	4.20

turn.

3.1. PSR J0613−0200

Figure 1 shows that this pulsar has a wide profile with three main components. Because of the short pulsar period and relatively high DM (Table 1) our observations are significantly smeared so the three components are not clearly resolved. However, the profile is very similar to that observed by Xilouris et al. (1998) at a similar frequency. Stairs et al. (1999) observe a quite different profile at 410 and 610 MHz, with the trailing component much stronger than the other two, showing that this component has a steeper spectrum. This frequency evolution is also consistent with the pulse profiles presented by Bell et al. (1997). At 610 MHz, Stairs et al. (1999) observe a reversal of circular polarization under this trailing component. This and the steep spectrum suggest that it may be 'core' emission despite its trailing location.

We observe weak linear polarization with a slow decrease in position angle across the profile and no significant circular polarization. Given the different frequency and time resolution, these results are not in disagreement with those observed by Stairs et al. (1999). Xilouris et al. (1998) did not show linear polarization in the figure for this pulsar, but give a fractional linear polarization of 26% and fractional circular polarization of −12% in their Table 1, both much higher than we observe (Table 2).

3.2. PSR J0711−6830

The pulse profile for this pulsar (Figure 2) has two broad and widely separated components connected by a bridge of emission. Profiles at frequencies between 430 and 1500 MHz published in the discovery paper (Bailes et al. 1997) show the leading component has a steeper spectrum than the trailing component. Our results show significant right-circular polarization across both components and linear polarization near the center of each component. Position angles differ by about 90° between the two components, but it is not clear if there is continuity between them. There are no previously published polarization measurements.

3.3. PSR J1045−4509

Figure 3 shows that this pulsar has a triangular shaped profile with a 50% width of 40° (Table 2). Most of the profile has weak left-circular polarization. The trailing part has significant linear polarization with approximately constant position angle. Again, there are

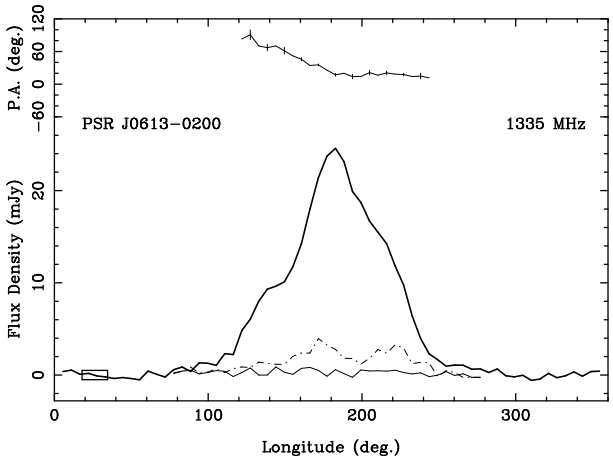

Fig. 1.— Polarization profiles for PSR J0613−0200 at 1335 MHz. In this and subsequent figures of this type the lower part gives the pulse profiles for total intensity I (thick line), linearly polarized intensity L (dot-dashed line) and circularly polarized intensity V (thin line). The abscissa is degrees of longitude where 360° equals the pulse period. The error box on the left-hand side of the profile has a width equal to the profile resolution (including dispersion smearing) and an amplitude of twice the baseline rms noise (i.e. $\pm 2\sigma$). In the upper part, the position angle of the linearly polarized emission is plotted where its uncertainty is less than 10°. Error bars ($\pm 2\sigma$) are given on every second point.

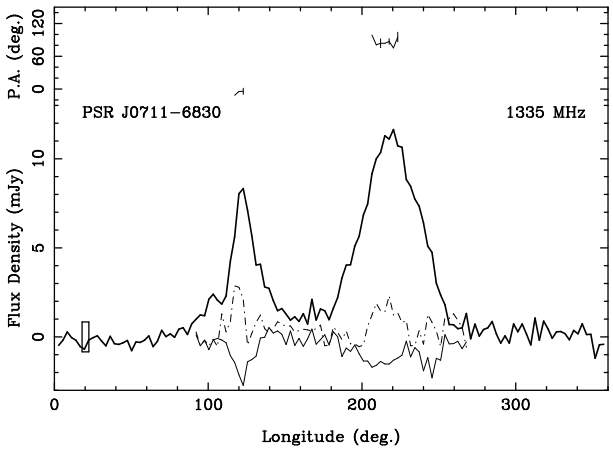

Fig. 2.— Polarization profiles for PSR J0711−6830 at 1335 MHz. See Figure 1 for details.

no previously published polarization measurements.

3.4. PSR J1603−7202

The only previously published profile for this pulsar is from the discovery paper (Lorimer et al. 1996) at 436 MHz which shows two barely resolved components. Figure 4 shows that the components become more separated at higher frequencies (in contrast to the frequency dependence observed in most normal pulsars) and that the leading component has a flatter spectrum.

The polarization properties of this pulsar, specifically the trailing component, are extraordinary. This component is one of the most highly circularly polarized broad-band radio continuum sources known, with a fractional circular polarization of more than 50% at 657 MHz and more than 65% at 1327 MHz. Weaker but still significant circular polarization is seen in the leading component, apparently with two sense reversals.

There is a clear but slightly smeared orthogonal flip in the linear polarization on the trailing edge of the first component at 1327 MHz with an accompanying dip in the linearly polarized intensity indicating overlap of two orthogonally polarized modes. Even when this is allowed for, the position angle variation across the pulse deviates from the simple RVM form. At 657 MHz, there may be two orthogonal flips of PA – it is difficult to tell because of the dispersion smearing. If so, the PA is approximately constant across the pulse.

3.5. PSR J1623−2631 (PSR B1620−26)

This three-component pulsar has high linear polarization in the leading component and moderate linear and right-circular polarization in the central component (Figure 5). There is some indication of an increasing PA with an orthogonal jump between the two components. These results are fully consistent with the results at 1408 MHz by Gould & Lyne (1998) and those at 610 MHz by Stairs et al. (1999), given the opposite sense of PA definition. In contrast, Xilouris et al. (1998) see a weakly polarized first component, decreasing PA through the central component, no orthogonal jump and left-circular polarization in the central component.

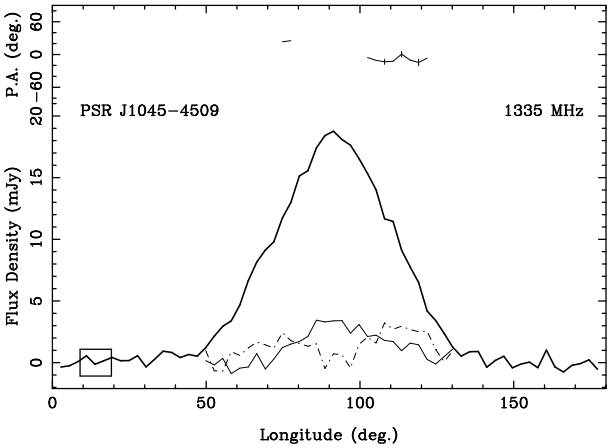

Fig. 3.— Polarization profiles for PSR J1045−4509 at 1335 MHz. See Figure 1 for details.

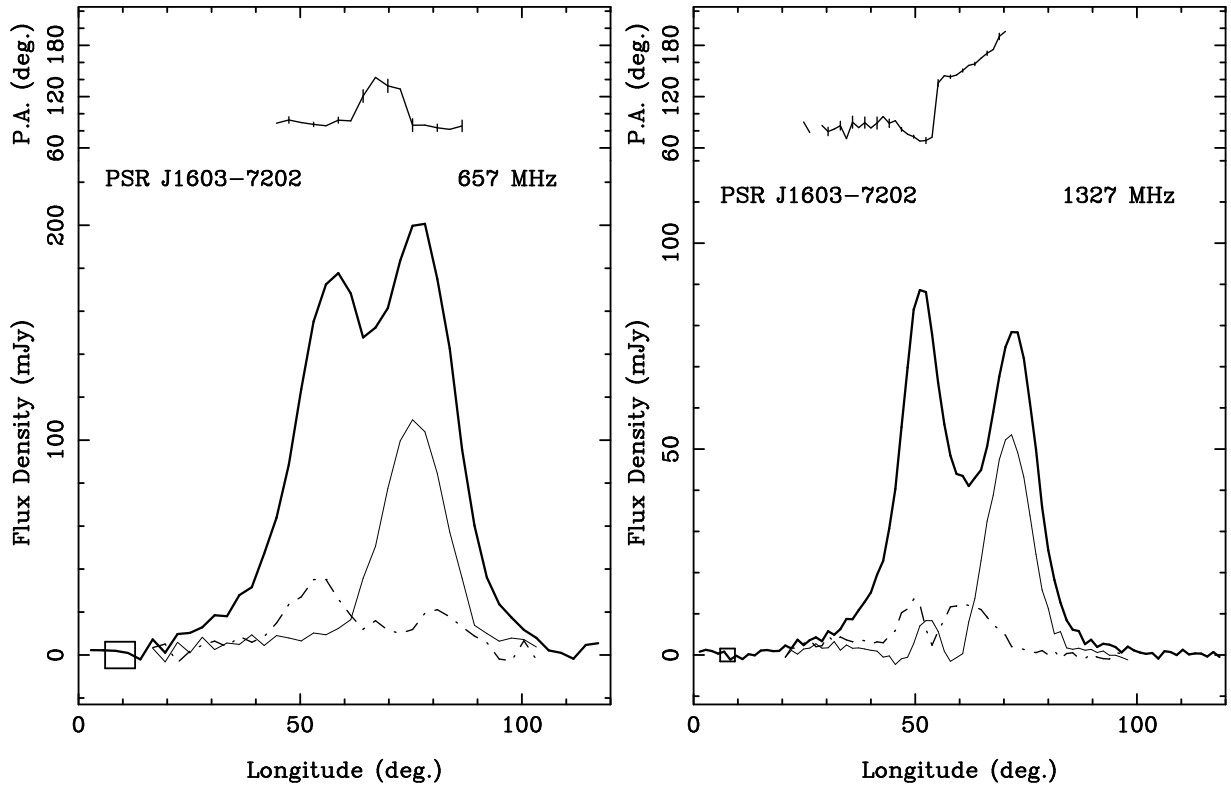

Fig. 4.— Polarization profiles for PSR J1603−7202 at 657 and 1327 MHz. See Figure 1 for details.

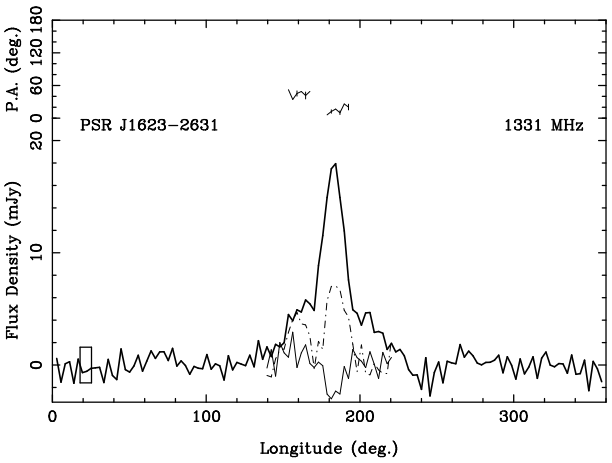

Fig. 5.— Polarization profiles for PSR J1623−2631 at 1331 MHz. See Figure 1 for details.

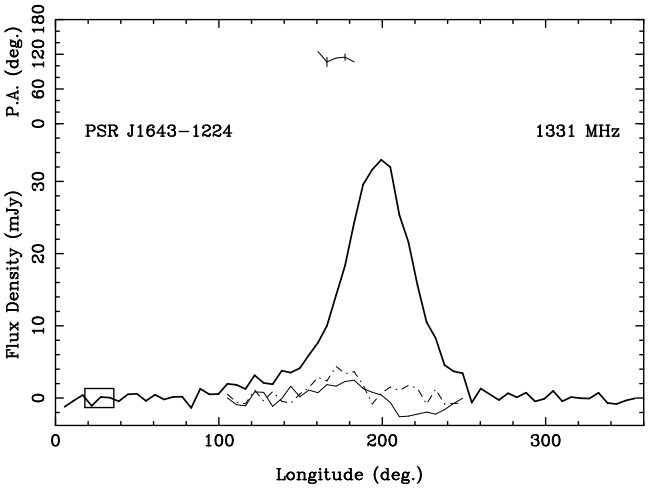

Fig. 6.— Polarization profiles for PSR J1643−1224 at 1331 MHz. See Figure 1 for details.

3.6. PSR J1643−1224

PSR J1643−1224 has a broad profile of almost gaussian shape except for an extended ramp of emission at the leading edge (Figure 6). There is some linear polarization in the first half of the pulse and weak circular polarization through the pulse with a sign reversal from left to right near the center. Within our uncertainties, the PA is constant across the linearly polarized part.

The 610-MHz data presented by Stairs et al. (1999) are consistent with those in Figure 6 except that they see no right-circular emission in the trailing half of the pulse. At 1410 MHz Xilouris et al. (1998) find linear polarization near the pulse peak with a slow decrease of PA and right-circular polarization through most of the profile.

3.7. PSR J2124−3358

Figure 7 presents the first polarization observations of this isolated millisecond pulsar (Bailes et al. 1997). The pulsar has an incredibly complex pulse profile with emission over essentially the whole pulse period. At least 12 pulse components can be identified in the 659-MHz profile which has higher signal-to-noise ratio than the 1327 MHz one. In fact this pulsar very likely emits at all rotational phases. This may be a serious problem for the polarization calibration as the true baseline for the Stokes parameters cannot be determined. We have taken the baseline to be the average level over 20° of longitude at the minimum of the Stokes I curve. If the pulsar has significant emission at this minimum phase, the polarization parameters derived here will be systematically biased, especially where the fractional polarization is low (cf. Rankin & Rathnasree 1997). The level of such emission can only be determined by pulse-phase resolved interferometric measurements. It is possible that this effect accounts for the small region near 130° longitude in the 1327-MHz profile where $L > I$, but this excess L may simply be due to non-random noise. The fact that $L \leq I$ everywhere else gives us some confidence that the effect of unpulsed emission, at both 659 and 1327 MHz, is small.

The components vary in relative strength between 659 and 1327 MHz, indicating a range of spectral indices. Figure 8 shows the variations in spectral index across the pulse profile. Absolute spectral indices cannot be estimated from these data as the observed signal strength is strongly affected by interstellar scintillation; in particular, the pulsar was exceptionally strong at the time of the 659 MHz observations. The two Stokes I profiles were normalised to the same area and aligned in longitude by matching the relatively isolated component near longitude 125° before computing the differential spectral index. This value was then added to

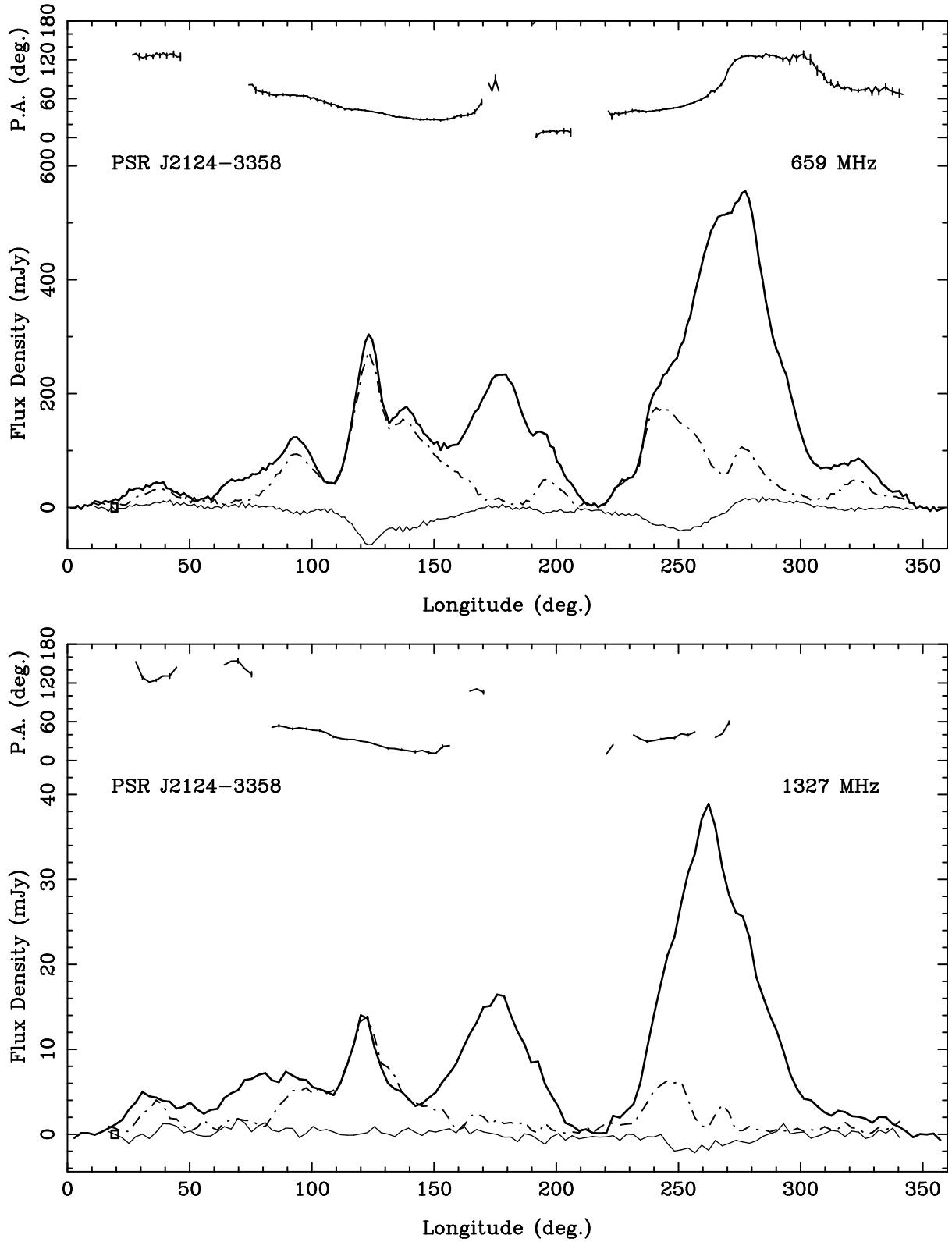

Fig. 7.— Polarization profiles of PSR J2124−3358 at 659 MHz and 1327 MHz. See Figure 1 for details.

the mean spectral index of −1.5 obtained by Toscano et al. (1998). The more positive values in regions of low-level emission may indicate a larger amount of unpulsed emission at the lower frequency. However, even discounting these regions, there is a remarkable variation in spectral index across the profile. The weak component near 140° has a very steep spectrum, whereas the central features around 180° and the leading side of the strong peak have much flatter spectra. This figure strongly suggests that individual components have distinct spectral indices, with regions of varying spectral index being due to overlapping components (cf. Kramer et al. 1994).

Portions of the profile are close to 100% linearly polarized, especially between 110° and 135° of longitude at both frequencies and on the leading edge of the main component (220° to 240°) at 659 MHz. On average, the fractional linear polarization is much higher at the lower frequency (Table 2). The variation of position angle across the profile is similar at the two frequencies and extremely complex. There may be orthogonal transitions at 1327 MHz around longitudes of 80° and 160°. The PA variations at 659 MHz between longitudes of 170° and 190° should be viewed with caution as the fractional polarization is low there.

At both frequencies there appears to be weak right-circular polarization in the leading part of the main peak, and at 659 MHz the highly linearly polarized component around 120° also has right-circular polarization. Overall, the circular polarization is much weaker than the linear, and weaker at 1327 MHz than at 659 MHz.

3.8. PSR J2129−5721

Figure 9 suggests that the mean pulse profile for this pulsar consists of a single broad gaussian-shaped peak with extended wings on both sides. However, especially at 659 MHz, the dispersion smearing is large and so narrower features may exist in the profile. Despite this smearing, it is clear that the profile has about 50% linear polarization at both frequencies, with a very slow decrease in PA across the profile. There is also relatively strong right-circular polarization (about 30%) through most of the profile, but with its peak somewhat delayed with respect to the total intensity profile.

3.9. PSR J2145−0750

The profile for PSR J2145−0750 shown in Figure 10 was obtained during a strong scintillation maximum and has a better signal-to-noise ratio than previously published polarization profiles (Xilouris et al. 1998; Stairs et al. 1999). The total intensity profile at 1335

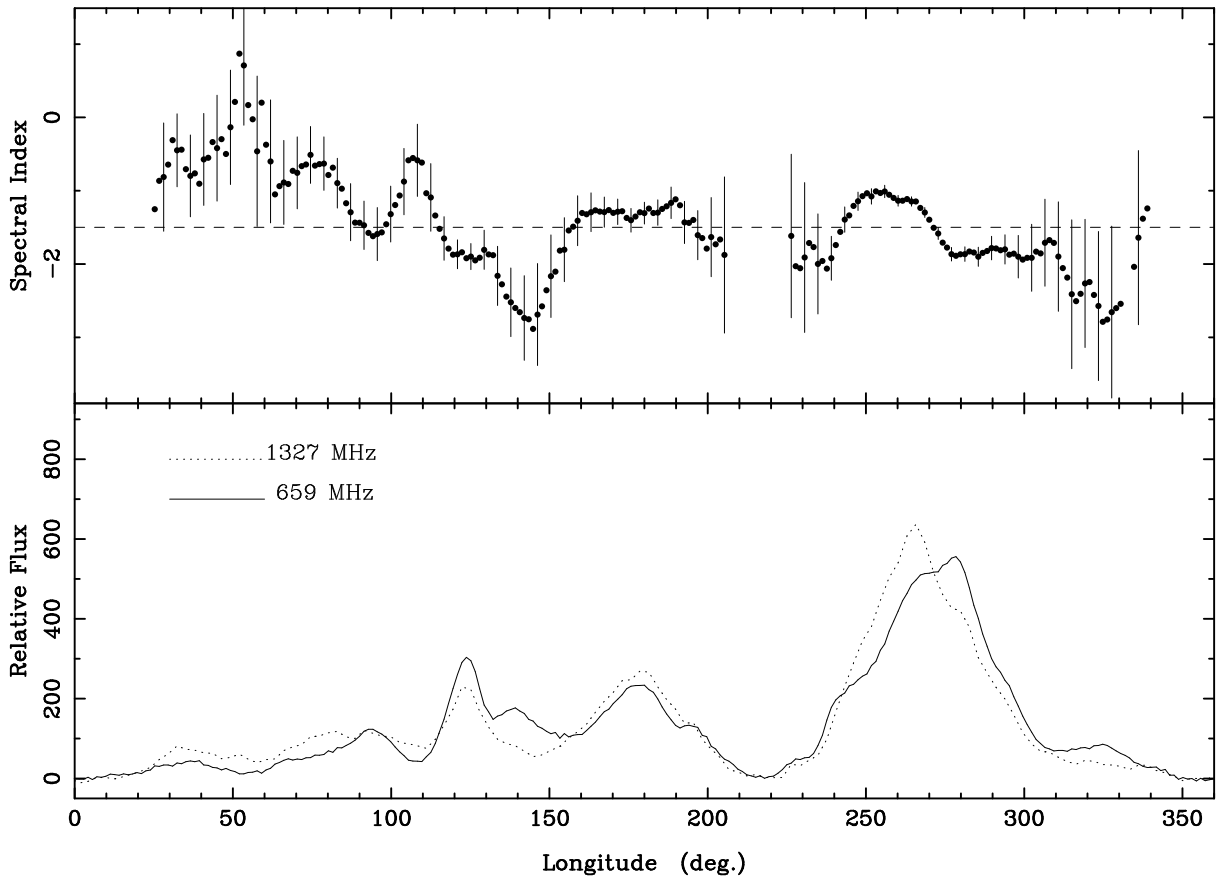

Fig. 8.— Distribution of spectral index across the pulse profile for PSR J2124-3358 derived from the 659 MHz and 1335 MHz data.

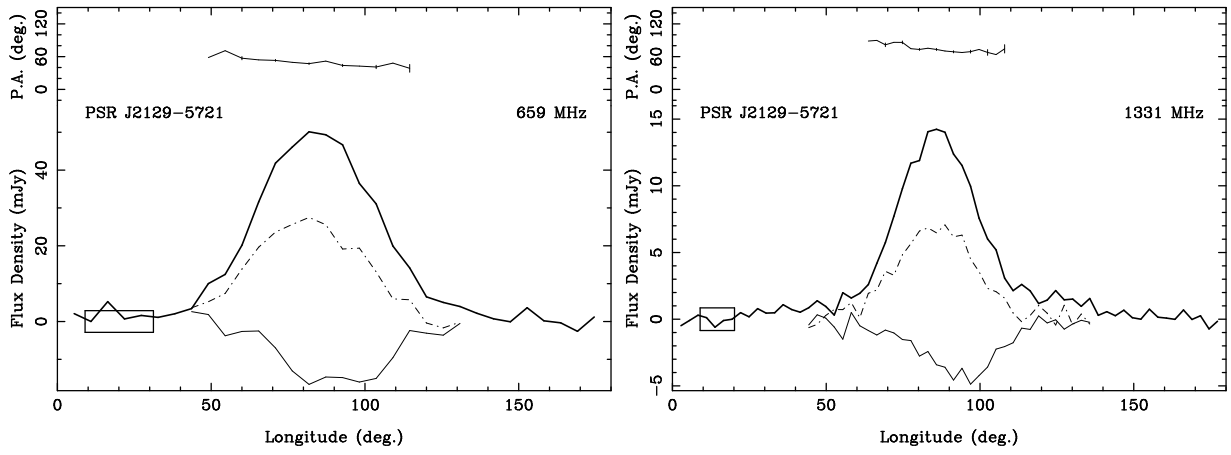

Fig. 9.— Polarization profiles for PSR J2129−5721 at 659 and 1331 MHz. See Figure 1 for details.

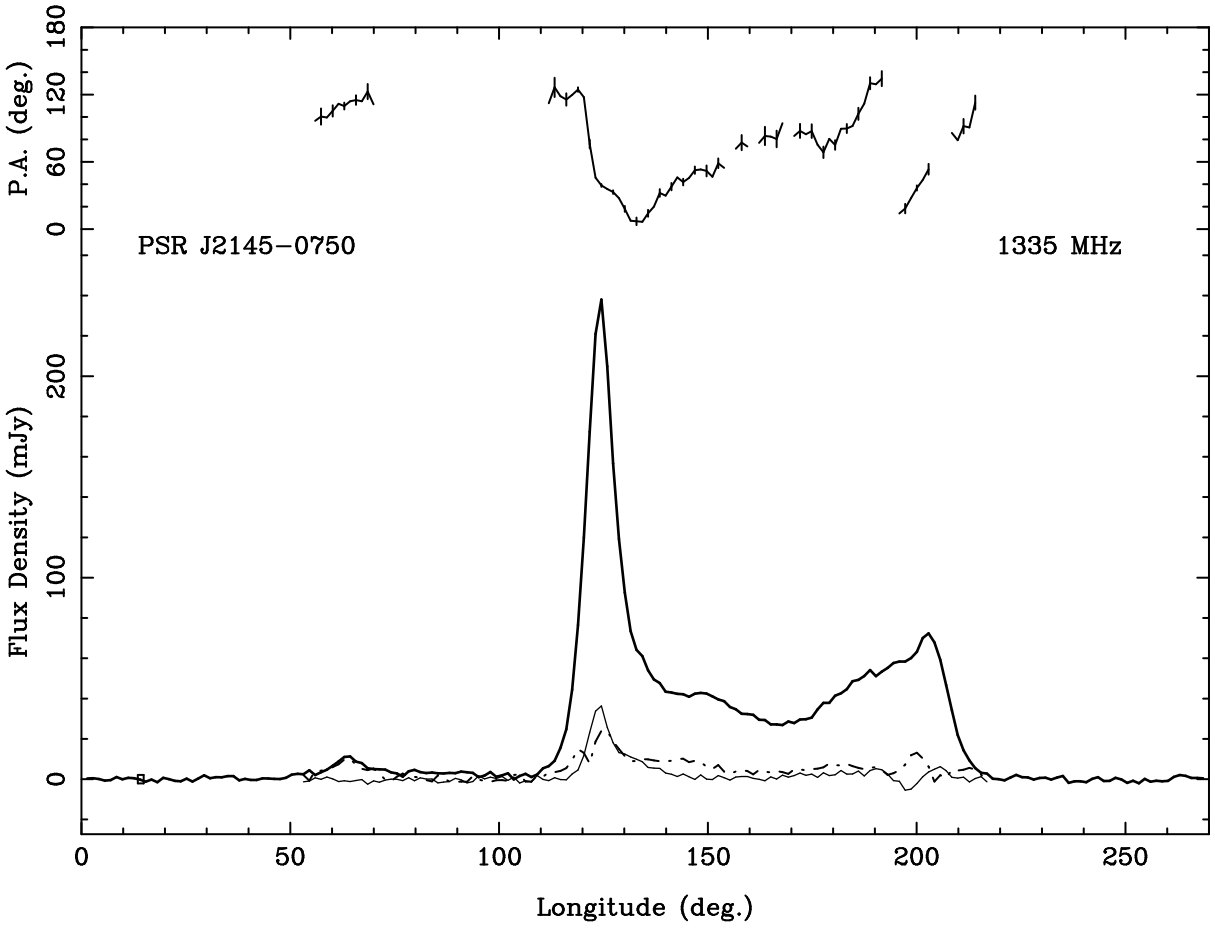

Fig. 10.— Polarization profiles for PSR J2145-0750 at 1335 MHz. See Figure 1 for details.

MHz consists of three main components with the central one dominating at this frequency. However, there is good evidence for at least two other pulse components between the main peak and the trailing component. Observations at frequencies between 102 MHz and 4850 MHz (Kramer et al. 1999a) show that the trailing component has a much steeper spectrum than the rest of the profile and dominates at low frequencies. Figure 10 shows that there is a weak but significant emission bridge between the leading and main component.

Although the weak leading component is essentially 100% polarized, linear polarization is relatively weak (but unambiguous) over most of the profile; the mean fractional linear polarization (Table 2) is 15%. There appears to be a rapid swing of position angle through the central component, but the higher time-resolution observations of Stairs et al. (1999) show that, at least at lower frequencies, there is an orthogonal PA jump at this longitude. There is also a rapid swing of PA in the trailing component, possibly also with an orthogonal jump. Significant circular polarization is observed in both components, with a sense reversal in the trailing component. Stairs et al. (1999) see a similar variation of circular polarization at 410 and 610 MHz, except that the sense of the sign reversal in the trailing component (left to right) is opposite to that seen in Figure 10. This may indicate a frequency evolution of the circular polarization behaviour at this longitude. Their 1414-MHz polarization profiles are consistent with those shown in Figure 10. Xilouris et al. (1998) also see strong linear polarization with an increasing PA in the weak leading component at 1410 MHz. However, their results for the stronger central and trailing half of the profile, with relatively strong linear polarization mimicing the total intensity profile and approximately constant PA, are inconsistent with those in Figure 10. Xilouris et al. (1998) also found a peak in circularly polarized intensity in the central component, but it is of opposite sign to that in Figure 10.

4. Rotation measures

Derived rotation measures for the nine MSPs are given in Table 3 along with the pulsar Galactic longitude, Galactic latitude and distance estimated from the DM using the NE2001 Galactic electron density model (Cordes & Lazio 2002). The mean line-of-sight component of the interstellar magnetic field, weighted by the local electron density, given by

$$\langle B_{||} \rangle = 1.232 \frac{\mathrm{RM}}{\mathrm{DM}} \, \mu\mathrm{G}, \tag{1}$$

where RM is in units of rad m^{-2} and DM is in cm^{-3} pc, is listed in the final column of the table. A positive $\langle B_{||} \rangle$ corresponds to a field pointing toward the observer. For PSR J1643−1224 there is a potential ambiguity owing to the possible presence of orthogonal modes; the PA differnce was computed from the first component. For the three pulsars where

measurements were available at both 20 cm and 50 cm (Table 2), the RM was computed from the observed PAs at the two frequencies. The RM increment corresponding to the 180° cycle of PA difference is ±20.1 rad m^2. The value closest to the weighted mean of the independent RMs determined at the two frequencies was chosen.

Two of these pulsars, J0711−6830 and J1643−1224, have surprisingly large values of $|\langle B_{||}\rangle|$, especially PSR J1643−1224 given its relatively large distance. In both cases, the $|\langle B_{||}\rangle|$ values are larger than for other pulsars located close to them on the sky (Han et al. 1999). These results will be further discussed in a forthcoming paper in the context of a large sample of pulsar RMs.

5. Discussion and Conclusions

In this paper we have presented pulse profiles and polarization parameters for nine southern MSPs, five of which had no previously published polarization data. New RM values are given for all nine pulsars. Notable results include the very high fractional circular polarization ($\sim 65\%$ at 1327 MHz) in the trailing component of PSR J1603−7202, and the extremely wide and complex pulse profile and polarization properties of PSR J2124−3358. Kramer et al. (1998) have argued that, on average, MSPs have profiles which are of similar complexity (quantified by the number of recognizable components) to those of normal pulsars. However, there is a tail to the distribution in MSPs exemplified by PSR J0473−4715 (Navarro et al. 1997), which has at least 10 components, and PSR J2124−3358 (Figure 7; at least 12 components) which is not present in normal pulsars; no normal pulsars have profiles as complex as these, even in data with high signal-to-noise ratio.

While many MSP profiles have the appearance of 'stretched' normal pulsar profiles, there are significant differences. One of the most important is the lack of frequency evolution in the spacing of pulse components (Kramer et al. 1999a). In most normal pulsars, the pulse components are more widely separated at lower radio frequencies, an observation often interpreted in terms of 'radius-to-frequency mapping' (e.g. Cordes 1978; Thorsett 1991). The results presented here confirm this lack of frequency evolution in MSP profiles. For example, Figure 8 shows that for PSR J2124−3358, although components are mostly overlapping, there is a clear correspondence of component locations at the two frequencies right across the profile. It is important to note however that this property is shared by normal pulsars with so-called 'interpulse' emission, including such well-known examples as the Crab pulsar (Moffett & Hankins 1999) and PSR B0950+08 (Hankins & Cordes 1981), suggesting a close link between the emission processes in MSPs and 'normal' interpulse pulsars.

Most MSP profiles do not fit easily into the 'core-cone' classification scheme (Rankin 1983; Lyne & Manchester 1988) or its extensions to multiple cones (e.g. Mitra & Deshpande 1999). Even when the profile has a shape similar to a classical 'triple', for example PSR J2145−0750 (Figure 10), the spectral properties of the central and outer components do not follow the patterns established for normal pulsars. For PSR J2124−3358 there is no identifiable 'core' component and there is no pattern suggesting multiple nested conal emission. While there do appear to be discrete quasi-gaussian components within the observed profile, a very large number of them would be required to model it and their amplitude and phase (longitude) shows no clear pattern. Rather, the profile seems more consistent with a random distribution of emission patches as advocated by Lyne & Manchester (1988). The spectral index variations shown in Figure 8 are consistent with different pulse components originating in spatially distinct emission regions.

The wide observed profiles of MSPs give a good opportunity to fit the RVM and hence to determine both the magnetic inclination α and the line-of-sight inclination ζ. Most normal pulsars have narrow profiles and only the impact parameter $\beta = \zeta - \alpha$ can be measured (cf. Lyne & Manchester 1988). In some MSPs, the observed PA variations follow the RVM quite well, especially at higher frequencies (e.g. Stairs et al. 1999; Lommen et al. 2000). However, in others, there are clear and sometimes large deviations (e.g. Arzoumanian et al. 1996; Navarro et al. 1997). Two pulsars in the present sample, PSRs J2124−3358 and 2145−0750, have sufficiently wide profiles to justify an attempt to fit the RVM. The results are shown in Figure 11.

While the overall PA variation for PSR J2124−3358 is approximately described by the RVM fit, it is clear that there are large and systematic deviations from the model fit. The parameters of this fit are $\alpha = 48^\circ \pm 3^\circ$ and $\zeta = 67^\circ \pm 5^\circ$, suggesting that emission is seen from both poles with impact parameters $\beta = 19^\circ$ and 65° respectively. However, there is a large covariance between α and ζ with only a small increase in χ^2 for α values between 20° and 60°. At these limits, the corresponding ζ values are 27° and 80° respectively. For small α, a one-pole interpretation is favoured. Given the poor quality of the fit, it is not at all clear what the true inclination angles for the two axes are. Certainly, the fact that emission is seen over most if not all of the pulse period suggests a one-pole, almost aligned model.

For PSR J2145−0750, if we assume there is an orthogonal flip near longitude 120° but not at 195°, we get the fit shown in Figure 11. This has $\alpha = 145^\circ \pm 12^\circ$ and $\zeta = 148^\circ \pm 12^\circ$. Again, there are systematic deviations from the fit and a large covariance between α and ζ, but the impact parameter $\beta \simeq 3^\circ$ is relatively well determined. This PA fit, the sense reversal of the circular polarization and the spectral behaviour all suggest that, despite the profile morphology, the trailing component is in fact central to the emission beam (cf. Stairs

Table 3: Rotation measures for southern millisecond pulsars

PSR	l (deg.)	b (deg.)	Dist. (kpc)	RM (rad m^{-2})	$\langle B_{\|\|} \rangle$ (μG)
J0613−0200	210.41	−9.30	1.71	$+19 \pm 14$	$+0.6 \pm 0.4$
J0711−6830	279.53	−23.28	0.86	$+67 \pm 23$	$+4.5 \pm 1.5$
J1045−4509	280.85	+12.25	1.96	$+82 \pm 18$	$+1.7 \pm 0.4$
J1603−7202	316.63	−14.50	1.17	$+20.1 \pm 0.5$	$+0.65 \pm 0.02$
J1623−2631	350.98	+15.96	1.80	-8 ± 20	-0.2 ± 0.4
J1643−1224	5.67	+21.22	2.41	-263 ± 15	-5.2 ± 0.3
J2124−3358	10.93	−45.44	0.27	$+1.2 \pm 0.1$	$+0.32 \pm 0.03$
J2129−5721	338.01	−43.57	1.36	$+37.3 \pm 0.2$	$+1.45 \pm 0.01$
J2145−0750	47.78	−42.08	0.57	$+12 \pm 8$	$+1.6 \pm 1.1$

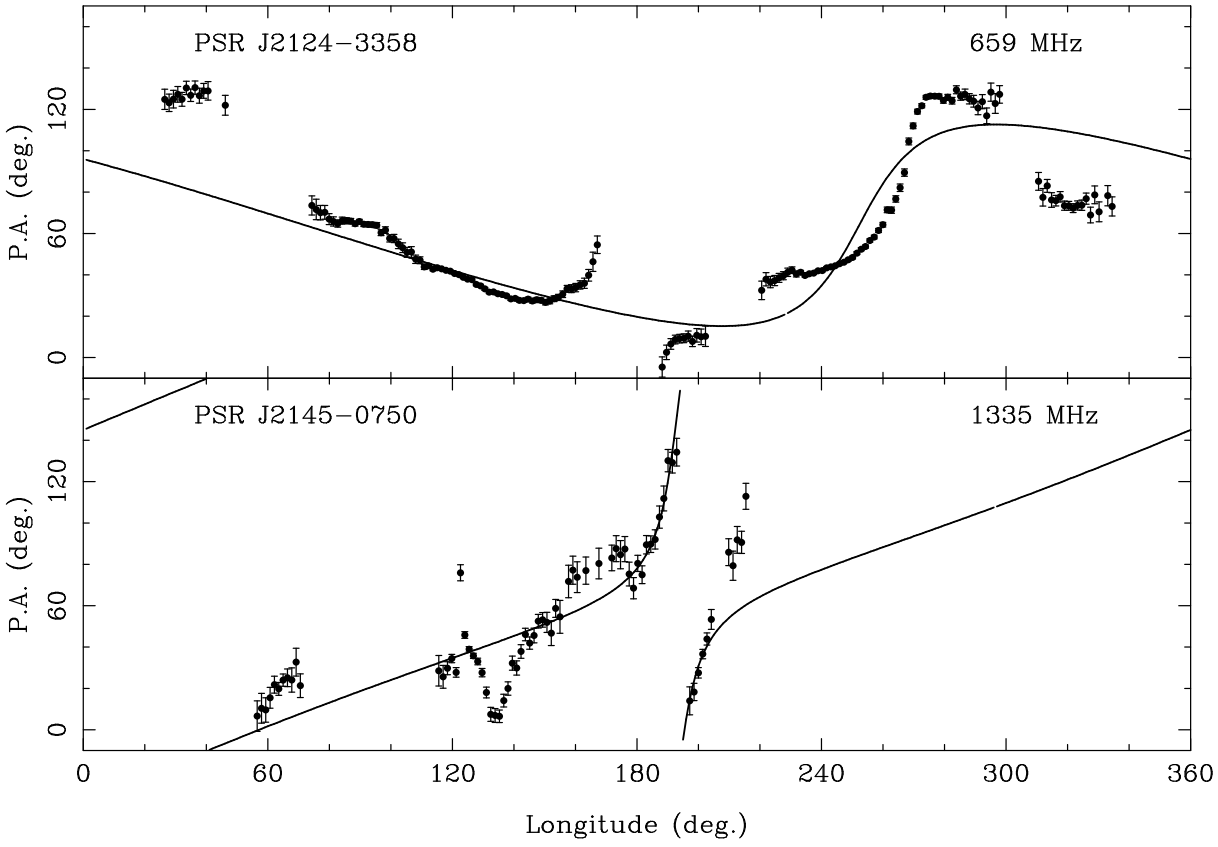

Fig. 11.— Rotating-vector model fits to observed position-angle variations for two pulsars.

et al. 1999). If we assume a second orthogonal jump at 195° the impact parameter increases to about 15°. However, this introduces a significant discontinuity in PA at this longitude, suggesting that this is not the correct interpretation.

If we accept that the trailing component is in fact central to the emission beam, the interpretation of the weak leading component becomes something of a problem. Xilouris et al. (1998) suggest that it is a 'precursor', analogous to that in the Crab pulsar. This is supported by its nearly 100% linear polarization. The emission bridge between the leading and strongest components suggests that all components are closely related and probably that all the emission orginates from one pole. This implies a very large effective pulse width, $2\Delta\phi \sim 300°$. For small β, $\sin(\rho/2) \simeq \sin(\Delta\phi/2)\sin(\alpha/2)$, where ρ is the true beam radius (cf. Lyne & Manchester 1988), giving $\rho \sim 68°$. This compares with a predicted value of 49° from the relation $\rho = 6.^{\circ}2\ P^{-1/2}$ (Biggs 1990).

For other pulsars in the sample, and indeed for most MSPs (Xilouris et al. 1998; Stairs et al. 1999), there is very little swing in PA across the the observed pulse components. Taken at face value, this implies large impact parameters and/or very small magnetic inclinations. Yet many of these pulsars have relatively narrow pulses, e.g. PSRs J0621+1002, J1518+4904 and J1713+0747 (Stairs et al. 1999). This implies a beam radius in the longitude direction much less than the apparent impact parameter, that is, a beam effectively elongated in the latitude direction (cf. Narayan & Vivekanand 1983). If these pulse components are part of a wide beam from magnetic field lines associated with one pole, as suggested for young 'interpulse' pulsars by Manchester (1996), intermediate magnetic inclinations and large impact parameters are possible. In this case, the implied emission altitudes relative to the light cylinder are much higher than those implied by observed pulse widths for normal pulsars. At these altitudes, there will be significant deviations of the magnetic field from a pure dipole form due to displacement and physical currents, providing a possible reason for the observed large PA deviations from RVM fits seen in millisecond pulsars.

It is also possible that these irregular PA variations result from very different magnetic field structures in MSPs. For example, Ruderman (1991) suggests that, during the spindown and subsequent recycling process, crustal plate movements result in highly distorted field structures. Accretion-induced field decay (e.g. Romani 1990) would also result in highly non-dipolar fields. Such field structures could also disguise or destroy the relatively consistent patterns of core and conal emission seen in most longer-period pulsars.

In general, our polarization results agree well with those of Stairs et al. (1999) when account is taken of the reversed PA convention in that paper. However, there are many discrepancies with results in the Xilouris et al. (1998) paper. It appears that their sign of Stokes V is systematically reversed. It is also probable that the higher and approximately

constant fractional linear polarization with nearly constant PA seen in a number of their figures results from errors in calibration rather than time variations in the polarization properties (cf. Stairs et al. 1999).

Acknowledgments

We thank the referee, Joanna Rankin, for helpful comments. JLH thanks the exchange program between CAS and CSIRO for support of the visits at the Australia Telescope National Facility in 1999 and 2000. His research is supported by the National Natural Science Foundation of China (10025313) and the National Key Basic Research Science Foundation of China (G19990756). The Australia Telescope is funded by the Commonwealth Government for operation as a National Facility managed by CSIRO.

REFERENCES

Arzoumanian, Z., Phillips, J. A., Taylor, J. H., & Wolszczan, A. 1996, ApJ, 470, 1111

Backer, D. C. 1976, ApJ, 209, 895

Bailes, M., Johnston, S., Bell, J. F., Lorimer, D. R., Stappers, B. W., Manchester, R. N., Lyne, A. G., D'Amico, N., & Gaensler, B. M. 1997, ApJ, 481, 386

Bell, J. F., Bailes, M., Manchester, R. N., Lyne, A. G., Camilo, F., & Sandhu, J. S. 1997, MNRAS, 286, 463

Biggs, J. D. 1990, MNRAS, 245, 514

Cordes, J. M. 1978, ApJ, 222, 1006

Cordes, J. M. & Lazio, T. J. W. 2002, http://xxx.lanl.gov/abs/astro-ph/0207156

Gould, D. M. & Lyne, A. G. 1998, MNRAS, 301, 235

Han, J. L. & Manchester, R. N. 2001, MNRAS, 320, L35

Han, J. L., Manchester, R. N., Lyne, A. G., & Qiao, G. J. 2002, ApJ, 570, L17

Han, J. L., Manchester, R. N., & Qiao, G. J. 1999, MNRAS, 306, 371

Han, J. L., Manchester, R. N., Xu, R. X., & Qiao, G. J. 1998, MNRAS, 300, 373

Hankins, T. H. & Cordes, J. M. 1981, ApJ, 249, 241

Helfand, D. J., Gotthelf, E. V., & Halpern, J. P. 2001, ApJ, 556, 380

Komesaroff, M. M. 1970, Nature, 225, 612

Kramer, M., Lange, C., Lorimer, D. R., Backer, D. C., Xilouris, K. M., Jessner, A., & Wielebinski, R. 1999a, ApJ, 526, 957

Kramer, M., Wielebinski, R., Jessner, A., Gil, J. A., & Seiradakis, J. H. 1994, A&AS, 107, 515

Kramer, M., Xilouris, K. M., Camilo, F., Nice, D., Lange, C., Backer, D. C., & Doroshenko, O. 1999b, ApJ, 520, 324

Kramer, M., Xilouris, K. M., Lorimer, D. R., Doroshenko, O., Jessner, A., Wielebinski, R., Wolszczan, A., & Camilo, F. 1998, ApJ, 501, 270

Lommen, A. N., Zepka, A., Backer, D. C., McLaughlin, M., Cordes, J. M., Arzoumanian, Z., & Xilouris, K. 2000, ApJ, 545, 1007

Lorimer, D. R., Lyne, A. G., Bailes, M., Manchester, R. N., D'Amico, N., Stappers, B. W., Johnston, S., & Camilo, F. 1996, MNRAS, 283, 1383

Lyne, A. G. & Manchester, R. N. 1988, MNRAS, 234, 477

Manchester, R. N. 1996, in Pulsars: Problems and Progress, IAU Colloquium 160, ed. S. Johnston, M. A. Walker, & M. Bailes (San Francisco: Astronomical Society of the Pacific), 193–196

Mitra, D. & Deshpande, A. A. 1999, A&A, 346, 906

Moffett, D. A. & Hankins, T. H. 1999, ApJ, 522, 1046

Narayan, R. & Vivekanand, M. 1983, A&A, 122, 45

Navarro, J. 1994, PhD thesis, California Institute of Technology

Navarro, J., Manchester, R. N., Sandhu, J. S., Kulkarni, S. R., & Bailes, M. 1997, ApJ, 486, 1019

Radhakrishnan, V. & Cooke, D. J. 1969, Astrophys. Lett., 3, 225

Radhakrishnan, V. & Deshpande, A. A. 2001, A&A, 379, 551

Rankin, J. M. 1983, ApJ, 274, 333

—. 1990, ApJ, 352, 247

—. 1993, ApJ, 405, 285

Rankin, J. M. & Rathnasree, N. 1997, J. Astrophys. Astr., 18, 91

Romani, R. W. 1990, Nature, 347, 741

Ruderman, M. 1991, ApJ, 382, 576

Stairs, I. H., Thorsett, S. E., & Camilo, F. 1999, ApJS, 123, 627

Staveley-Smith, L., Wilson, W. E., Bird, T. S., Disney, M. J., Ekers, R. D., Freeman, K. C., Haynes, R. F., Sinclair, M. W., Vaile, R. A., Webster, R. L., & Wright, A. E. 1996, Proc. Astr. Soc. Aust., 13, 243

Stinebring, D. R., Cordes, J. M., Rankin, J. M., Weisberg, J. M., & Boriakoff, V. 1984, ApJS, 55, 247

Thorsett, S. E. 1991, ApJ, 377, 263

Thorsett, S. E. & Stinebring, D. R. 1990, ApJ, 361, 644

Toscano, M., Bailes, M., Manchester, R., & Sandhu, J. 1998, ApJ, 506, 863

Xilouris, K. M., Kramer, M., Jessner, A., von Hoensbroech, A., Lorimer, D., Wielebinski, R., Wolszczan, A., & Camilo, F. 1998, ApJ, 501, 286